The Cryosphere Discuss., 9, 5521–5554, 2015
www.the-cryosphere-discuss.net/9/5521/2015/
doi:10.5194/tcd-9-5521-2015

The Cryosphere Discussions
Open Access

Seasonal sea ice predictions for the Arctic based on assimilation of remotely sensed observations

F. Kauker[1,3], T. Kaminski[2,a], R. Ricker[3], L. Toudal-Pedersen[4], G. Dybkjaer[4], C. Melsheimer[5], S. Eastwood[6], H. Sumata[3], M. Karcher[1,3], and R. Gerdes[3,7]

[1]OASys, Tewessteg 4a, 20249 Hamburg, Germany
[2]The Inversion Lab, Tewessteg 4a, 20249 Hamburg, Germany
[3]Alfred Wegener Institute, Bussestr. 24, 27570 Bremerhaven, Germany
[4]Danish Meteorological Institute, Lyngbyvej 100, 2100 Copenhagen, Denmark
[5]University of Bremen, Institute for Environmental Physics, Otto-Hahn-Allee 1, 28359 Bremen, Germany
[6]The Norwegian Meteorological Institute, Blindern 43, 0313 Oslo, Norway
[7]Jacobs University, Campus Ring 1, 28759 Bremen, Germany
[a]previously at: FastOpt, Hamburg, Germany

Received: 8 September 2015 – Accepted: 22 September 2015 – Published: 16 October 2015

Correspondence to: F. Kauker (frank@oasys-research.com)

Published by Copernicus Publications on behalf of the European Geosciences Union.

Abstract

The recent thinning and shrinking of the Arctic sea ice cover has increased the interest in seasonal sea ice forecasts. Typical tools for such forecasts are numerical models of the coupled ocean sea ice system such as the North Atlantic/Arctic Ocean Sea Ice Model (NAOSIM). The model uses as input the initial state of the system and the atmospheric boundary condition over the forecasting period. This study investigates the potential of remotely sensed ice thickness observations in constraining the initial model state. For this purpose it employs a variational assimilation system around NAOSIM and the Alfred Wegener Institute's CryoSat-2 ice thickness product in conjunction with the University of Bremen's snow depth product and the OSI SAF ice concentration and sea surface temperature products. We investigate the skill of predictions of the summer ice conditions starting in March for three different years. Straightforward assimilation of the above combination of data streams results in slight improvements over some regions (especially in the Beaufort Sea) but degrades the over-all fit to independent observations. A considerable enhancement of forecast skill is demonstrated for a bias correction scheme for the CryoSat-2 ice thickness product that uses a spatially varying scaling factor.

1 Introduction

The state of the Arctic climate system is rapidly changing (Stroeve et al., 2007). This change is impacting ecosystems, coastal communities, and economic activities. In this context, high-quality predictions of the ice conditions are of paramount interest (AMAP, 2011). This topic is addressed, for example, by the Sea Ice Outlook (http://www.arcus.org/sipn/sea-ice-outlook). In this activity, various research groups are applying different approaches to predict the Arctic summer minimum sea ice extent based on the state of the Arctic system at the beginning of the melting season (around May/June). The range of approaches extends from heuristic techniques, sta-

tistical models, coupled sea ice ocean models to fully coupled models of the atmosphere sea ice ocean system. An analysis of Stroeve et al. (2014) shows that none of the approaches outperforms its competitors. In general, however, due to the rapid transition of the Arctic system, the validity of heuristic and statistical relationships derived from the past may be limited (Holland and Stroeve, 2011). In contrast, dynamical models that include all relevant processes should be able to handle such transitions although the values of their process parameters are based on past observations. While some of the dynamical models (fully coupled models) include an atmospheric component (see, e.g. Wang et al., 2013; Chevallier et al., 2013; Sigmond et al., 2013), other models are restricted to the sea ice–ocean system (sea ice–ocean models, see, e.g. Zhang et al., 2008; Lindsay et al., 2012; Massonnet et al., 2015). The latter class of models are driven with prescribed atmospheric fields, provided, e.g., by atmospheric forecasting/numerical weather prediction centres. These fields are typically constrained by a range of atmospheric observations and are thus probably more realistic than those computed by a fully coupled model. On the other hand, fully coupled models allow a consistent simulation of the feedback loops through all components of the atmosphere–sea ice–ocean system.

Predictions by a dynamical model depend on the state of the system at the beginning of the simulation period (initial state). Previous studies have highlighted the role of the initial ice thickness distribution (Kauker et al., 2009; Holland and Stroeve, 2011; Lindsay et al., 2012; Chevallier and Salas-Mélia, 2012) for the forecast quality. Systematic use of observational information in a data assimilation system can help to derive an improved estimate of the initial state (Lindsay et al., 2012; Chevallier et al., 2013; Yang et al., 2014; Massonnet et al., 2015).

The present article describes the construction of an assimilation and prediction system of the Arctic sea ice conditions. Observational data streams for such a prediction system have to be available near real time. We use four data streams which fulfill this requirement, namely, the OSI SAF sea ice concentration and sea surface temperature products, a snow depth product provided by the University of Bremen, and the CryoSat-

2 ice thickness product derived at the Alfred Wegener Institute (AWI). The availability of the above data streams is limited to the period from 2012 to 2014. Also there is only one single two month period per year (March and April) for which the CryoSat-2 product is currently available (and note that the followup version covers October to April/May). We thus restrict our study to assimilation of the above four data streams in the spring of each of the three years and to prediction of the ice conditions in the following summer.

The assimilation system is built around the regional North Atlantic/Arctic Ocean Sea Ice Model (NAOSIM, Gerdes et al., 2003; Kauker et al., 2003). Initial tests indicated that the model was not sufficiently calibrated to achieve the required high simulation quality. Hence, in a preliminary step, some of the process parameters in the formulation of our model were adapted to better match observations over the 19 year period from 1990–2008. Furthermore, it turned out that the assimilation system was not capable of integrating the information in the above-mentioned CryoSat-2 ice thickness product to a sufficient degree. Through a set of additional assimilation experiments, we were able to develop a so-called bias correction scheme that allowed to take full advantage of this data stream.

2 Methods

2.1 Assimilation

NAOSIMDAS is a variational assimilation system that estimates a control vector $\boldsymbol{x}$ through minimisation of a cost function $J(x)$ that quantifies the fit to all observations plus the deviation from prior knowledge on x:

$$J(\boldsymbol{x}) = \frac{1}{2}\left[(M(\boldsymbol{x}) - \boldsymbol{d})^T \mathbf{C}(\boldsymbol{d})^{-1}(M(\boldsymbol{x}) - \boldsymbol{d}) + (\boldsymbol{x} - \boldsymbol{x}_0)^T \mathbf{C}(\boldsymbol{x}_0)^{-1}(\boldsymbol{x} - \boldsymbol{x}_0)\right] \quad (1)$$

where M denotes the model, considered as a mapping from the control vector to observations, d the observations with data uncertainty covariance matrix $\mathbf{C}(d)$, $\boldsymbol{x}_0$ the vector

of prior values of the control variables with uncertainty covariance matrix $\mathbf{C}(\boldsymbol{x}_0)$, and the superscript T is the transposed. The control variables are typically a combination of the initial state, the atmospheric forcing and the process parameters. In this study the control vector is restricted to the model's initial state.

The data uncertainty $\mathbf{C}(d)$ reflects the combined effect of observational $\mathbf{C}(d_{\text{obs}})$ and model error $\mathbf{C}(d_{\text{mod}})$:

$$\mathbf{C}(d)^2 = \mathbf{C}(d_{\text{obs}})^2 + \mathbf{C}(d_{\text{mod}})^2. \quad (2)$$

$\mathbf{C}(d_{\text{mod}})$ captures all uncertainty in the simulation of the observations except for the uncertainty in the control vector, because this fraction of the uncertainty is explicitly addressed by the assimilation procedure through correction of the control vector. In this study we assume that $\mathbf{C}(d_{\text{obs}})$ considerably exceeds $\mathbf{C}(d_{\text{mod}})$ and neglect the latter. The non-diagonal elements of $\mathbf{C}(d_{\text{obs}})$ are assumed to be zero (no correlation of the uncertainty of different components of the observation vector). The same is assumed for the prior uncertainty, $\mathbf{C}(\boldsymbol{x}_0)$.

Technically, the cost function is minimised by a gradient algorithm. The algorithm iteratively uses the gradient of the cost function, which is efficiently provided by so-called adjoint code of NAOSIM (Kauker et al., 2009) generated by the automatic differentiation tool TAF (Giering and Kaminski, 1998).

2.2 Observations

This study assesses the potential of remotely sensed observations of the sea ice and ocean system to increase the skill of seasonal predictions of that system through initialisation of NAOSIM. For this purpose, the data streams have to be available operationally or have to become operational in the near future. EUMETSAT's Ocean and Sea Ice Satellite Application Facility (OSI SAF) operationally provides sea ice concentration and sea surface temperature. Currently available sea ice thickness products are derived from SMOS (Kaleschke et al., 2012) and CryoSat-2 (Wingham et al., 2006). While the SMOS product copes better with thin ice, CryoSat-2 copes better with thick

ice. As thinner ice tends to be completely melted in summer, we expect the information on thicker ice to be more important in our context and select a CryoSat-2 product, namely the one provided by the Alfred Wegener Institute (Ricker et al., 2014). A snow depth product is provided by the University of Bremen. The above data sets allow to perform data assimilation experiments starting in March for each of the years 2012 to 2014 and will be described in more detail below.

As mentioned above, a preliminary step consists in the calibration of the model against observations (labeled historical) over the period from 1990–2008 (calibration period). Operational availability of the data products was obviously not required. We use remotely sensed sea ice concentration provided by OSI SAF, sea ice thickness from ICESat provided by JPL, and two drift products. A detailed description of the products is provided below.

2.2.1 Historical data sets

The only data stream available all year for the entire calibration period is the reprocessed OSI SAF ice concentration product (Eastwood et al., 2015). It is available in daily temporal and 10 km spatial resolution and includes spatially and temporally varying uncertainty estimates $\sigma(d_{\text{obs}})$ as required by Eq. (1).

The ICESat-JPL ice thickness (available in February/March and October/November from 2003 to 2008) is available at about monthly temporal and 25 km spatial resolution and does not include an uncertainty estimate. Kwok and Cunningham (2008) estimate a mean error of about 50 cm, corresponding to a relative error of about 40 %. For the present study we thus use 40 % relative uncertainty but completely exclude observations below 1 m (as the uncertainty increases for thin ice). ICESat-JPL thickness data are omitted where the difference to the ICESat thickness product provided by the Goddard Space Flight Center (ICESat-GSFC, Zwally et al., 2008) exceeds 40 cm.

The OSI SAF winter ice drift product (Lavergne et al., 2010) is available at bi-daily temporal and 62.5 km spatial resolution but does not include uncertainty estimates. In the present study we use the monthly mean value and corresponding uncertainty

estimates of Sumata et al. (2014). This data set covers the winter season (October to April) for the period from October 2003 to December 2006.

The KIMURA summer ice drift product (Kimura et al., 2013) is available at daily temporal and 75 km spatial resolution and does not include uncertainty estimates either. As for the winter ice drift we use monthly mean values and uncertainty estimates derived by Sumata et al. (2015). The data set covers the summer months May to July for the years 2003 to 2007.

2.2.2 Operational products

The operational OSI SAF ice concentration product is available at daily temporal and 10 km spatial resolution and based on the combination of the Comiso frequency mode (CF) algorithm and the Bristol (BR) algorithm. Both products use the 19 and 37 GHz channels, with respective native resolutions (footprints) of about 60 and 30 km. The product does include discrete quality flags (while the followup product will provide an uncertainty estimate). For this study an uncertainty estimate is derived by a procedure that was developed within the Sea Ice project (http://esa-cci.nersc.no/) of ESA's Climate Change Initiative (SICCI). The procedure considers the algorithmic uncertainty and a so-called "smearing uncertainty". The algorithmic uncertainty σ_a, i.e. the uncertainty derived by propagating radiometric noise through the algorithm, is only available in the re-processed OSI SAF concentration product. As it hardly exceeds 6 percentage points in the re-processed product, this value is used for all grid cells and all days as a conservative estimate of the algorithmic uncertainty. The (spatially and temporally variable) smearing uncertainty reflects the combination of two sources of error: first, the error caused by providing a 10 km product from coarser native resolutions, and, second, the error caused by combining channels with different footprints. An estimate of this uncertainty is calculated by comparing high resolution SIC aggregated to 10 km resolution (reference) and that computed at the SSMI footprints using both, the CF and the BR algorithm. The empirical formula $\sigma_s = \sqrt{\mathrm{SD}}/2.2$ (see Fig. 1) provides an approximation of the root mean squared difference as a function of the 3×3 standard deviation

SD (grid point and eight surrounding grid points). Assuming the independence of both uncertainties the total observational uncertainty is given by $\sigma(d_{\mathrm{obs}}) = \sqrt{\sigma_a^2 + \sigma_s^2}$.

The OSI SAF high latitude SST product (Eastwood, 2011a) has a resolution of 5 km and is produced twice daily at 00:00 and 12:00 UTC. It covers the Atlantic Ocean from 50 to 90° N, with the exception of areas covered by ice or clouds. A constant uncertainty of 0.5 K is applied (Eastwood, 2011b).

AWI's CryoSat-2 ice thickness product is provided on a monthly temporal and 25 km spatial grid, including an ice type classification into first-year and multi-year ice, which is adopted by the OSI SAF ice type product (Eastwood et al., 2015). The main source of systematic uncertainty in the CryoSat-2 ice thickness retrieval is due to the selection of the return-power threshold value in the retracker algorithm (Ricker et al., 2014). This algorithm is essential to derive the actual range measurement from the radar-return signal. Therefore, a return-power threshold is used at the first maximum of the echo power distribution to retrieve the range estimate, which is then used to calculate sea ice thickness. In order to estimate this algorithm uncertainty, we use a small ensemble of ice thickness values retrieved by Ricker et al. (2014) for three different thresholds with 40, 50, and 80 % (range of value in the literature) of the first maximum of the radar echo power. For the present study we use the ice thickness retrieved with the 50 % threshold as it provides the best match to the ice thickness, simulated by (the recalibrated version of) NAOSIM. The standard deviation of this ensemble over first-year ice is about 20 % and over multi-year ice about 50 %. We use these two values as relative uncertainties of the ice thickness for the respective ice types.

A snow depth product on the NAOSIM grid is provided by the University of Bremen. It has a daily temporal resolution and includes uncertainty estimates. The basis is an algorithm following Markus and Cavalieri (1998), which is applicable to level ice under non-melting conditions. To mask out areas where these conditions are not met, the radar backscatter at 5.3 GHz (C band) is used as it is increased in melting conditions and for rough ice. Here, a threshold of −13 dB for the normalised radar backscattering cross section is used. On first-year ice the maximum of the following three uncer-

tainty estimates is used: (1) a value of 6 cm as estimated from a comparison with the NASA ice bridge mission (Kurtz et al., 2013a, b), (2) a value derived by Gaussian error propagation from the radiometric error of the input data (satellite brightness temperatures) and the uncertainty of the retrieval parameters, (3) the standard deviation of the most recent five days of retrieved snow depths. On multi-year ice and under melting-conditions a very large uncertainty of 5 m is applied.

2.3 NAOSIM

NAOSIMDAS is constructed around the North Atlantic/Arctic Ocean Sea Ice Model (NAOSIM) (Kauker et al., 2003). The model is derived from version 2 of the Modular Ocean Model (MOM-2) of the Geophysical Fluid Dynamics Laboratory (GFDL). The version of NAOSIM used here has a horizontal grid spacing of 0.5° on a rotated spherical grid. The rotation maps the 30° W meridian onto the equator and the North Pole onto 0° E. In the vertical it resolves 20 levels, their spacing increasing with depth. The ocean model is coupled to a sea ice model with viscous-plastic rheology (Harder, 1996). At the open boundary near 50° N the barotropic oceanic transport is prescribed from a coarser resolution version of the model that covers the whole Atlantic north of 20° S (Köberle and Gerdes, 2003).

The state of the model comprises five fields, namely ocean temperature and salinity (velocities are diagnostic), ice thickness and concentration (drift is diagnostic) as well as snow depth. These five fields form the control vector $\boldsymbol{x}$ in our assimilation system described in Sect. 2.1.

In contrast to the version described by Kauker et al. (2003), the present version uses a modified atmospheric forcing data set consisting of 10 m-wind velocity, 2 m-air temperature, 2 m-specific humidity, total precipitation, and downward solar and thermal radiation. For the period from 1979 to 2010 the forcing is taken from the National Center for Environmental Prediction (NCEP) Climate Forecast System Reanalysis (NCEP-CFSR) (Saha and et al., 2010) and for the period from 2011 to the end of 2014 from the NCEP Climate Forecast System version 2 (CFSv2) (Saha and et al., 2014).

The initial state of 1 January 1980 is taken from a hindcast from 1 January 1948 to 31 December 1979. As in Kauker et al. (2003) this hindcast run was forced by the NCEP/NCAR reanalyses (Kalnay et al., 1996) and, in turn, initialized from PHC Steele et al. (2001) (ocean temperature and salinity), zero snow depth, and a constant ice thickness of 2 m with 100 % ice concentration where the air temperature is below the freezing temperature of the ocean's top layer.

The above-described historical data sets were used to estimate a sub-set of the sea ice–ocean model's process parameters, with focus on parameters that influence the ice dynamics. These are the atmospheric drag coefficient (cdair), the oceanic drag coefficient (cdwat), the ice strength parameter (p^*), the parameter that determines the dependence of the ice pressure on the ice concentration (c^*) and the parameter that determines the ellipsoid of the rheology (eccen) that represents the ratio of the normal stress and the shear stress. Additionally the vertical ocean tracer mixing parameter kappa_h is adjusted.

In our model we observe a memory of the Arctic sea ice system in the range of 7 to 10 years. We thus performed model runs over the 29 year period from January 1980 until end of December 2008, skipped the first 10 years, and evaluated the (quasi) equilibrium response for the remaining 19 years (calibration period).

The performance of the model is evaluated in terms of its weighted fit (as defined by the first term of Eq. 1) to observed sea ice concentration, ICESat-JPL ice thickness, winter ice drift from OSI SAF, and summer ice drift from KIMURA as described above (Table 1). For the computation of the total misfit, each term is normalised to yield a value of 1 for the standard configuration, in order to achieve an equal weighting of the terms despite their varying number of observations. By this procedure we find a configuration that reduces the misfit of ice thickness and ice drift strongly but increases the misfit of ice concentration, especially in winter where the ice margin is located too far south. Because here we are interested in the seasonal predictions of summer ice conditions, this deficit is tolerated. In the following we call this configuration newNAOSIM.

PIOMAS 2.1 (Zhang and Rothrock, 2003), an Arctic sea ice–ocean model which uses Optimal Interpolation to assimilate ice concentration and sea surface temperature, is often used as a reference, because it is well validated (see e.g. Schweiger et al., 2011). Its misfit to ice thickness and ice drift is added to Table 1. NewNAOSIM performs slightly worse than PIOMAS2.1 with respect to ice thickness and better with respect to ice drift.

Another reference is TOPAZ4 (Sakov et al., 2012) which uses an Ensemble Kalman filter to assimilate satellite observed sea level anomaly, sea surface temperature, sea ice concentrations from AMSR-E (NSIDC), sea ice drift products from CERSAT and Coriolis in-situ temperature and salinity profiles. NewNAOSIM outperforms TOPAZ4 with respect to ice thickness and ice drift (Table 1).

The deviations of the climatologies of newNAOSIM, PIOMAS2.1, and TOPAZ4 from the IceSat-JPL climatology (Fig. 2) (from 2003 to 2008) reveal similarities between newNAOSIM and PIOMAS2.1 (compare Schweiger et al. (2011), Fig. 6). Both show too thick ice in the Beaufort Sea in February/March and too thin ice north of the Canadian Archipelago and north of Greenland and north of Fram Strait in February/March and October/November when compared to ICESat-JPL. This is very remarkable because both simulations differ in terms of model formulation and parameterizations and atmospheric forcing (NCEP-CFSR in case of NAOSIM and NCEP in case of PIOMAS2.1 which differ considerably for some variables, see e.g. Lindsay et al., 2014). In contrast to newNAOSIM and PIOMAS2.1 in February/March TOPAZ4 exhibits a large negative bias in the Eurasian Basin, especially north of Fram Strait. In October/November TOPAZ4 is closer to newNAOSIM and PIOMAS2.1. The ice thickness of newNAOSIM, PIOMAS2.1, and TOPAZ4 for September 2007 is shown in Fig. 3. Although newNAOSIM uses no assimilation of sea ice or ocean observations the pattern of the sea ice cover deviates not stronger from PIOMAS2.1 and TOPAZ4 than PIOMAS2.1 deviates from TOPAZ4 (although both models use assimilation of ice concentration from NSIDC).

The sea ice area in September for newNAOSIM is in good agreement with three different observational data streams (Fig. 4). The minima in 2007 and 2013 and the

long-term trend are captured by the model. The largest deviations occur between 1998 and 2003 where the model overestimates the sea ice area. As this strong deviation is absent when forced with the NCEP reanalysis (not shown) this can be attributed to deficits in the NCEP-CFSR surface forcing.

3 Experiments

In this section three different sets of experiments are described: The first set performs a straightforward initialisation through simultaneous assimilation of all four data streams described in Sect. 2.2.2. The second set uses all data streams but the ice thickness, and aims at reconstructing ice thickness fields that are consistent with those three data streams and the model. Based on these reconstructed fields a bias correction scheme for CryoSat-2 ice thickness is derived and applied in the final set of experiments.

3.1 Straightforward initialisation

We assimilate CryoSat-2 ice thickness (50 % retracker threshold), ice concentration, snow depth and SST with uncertainties as described in Sect. 2.2.2. We perform three experiments, one for each of the years for 2012 to 2014, and in each year use a two-month assimilation window from 1 March until 30 April. The costfunction contribution from Cryosat-2 ice thickness, the data stream in the focus of this study, is based on monthly-mean values, while the contributions from the other data streams are based on daily values. This would result in a substantially lower weight of the ice thickness contribution. We artificially increase its weight by a factor of 180 to ensure that this contribution has the same order of magnitude as the other terms.

In all three experiments, the iterative minimisation procedure of our assimilation system achieves a substantial reduction of the cost function gradient in 50 to 70 iterations. For each experiment, Fig. 5 shows the total costfunction and the contributions of all four data streams and the prior separately before (a priori) and after the last iteration (a pos-

teriori). The contributions from ice thickness and snow depth are strongly decreased, and for ice concentration and SST the decrease is slightly weaker.

For each experiment, the March ice thickness of CryoSat-2 of the prior run (with a priori control vector) and the posterior run (with a posteriori control vector) are shown in Fig. 6. The Beaufort Sea, the East Siberian Sea and in the Kara and Laptev Seas exhibit the largest change from prior to posterior. In March 2014, both prior and posterior simulations show (consistent with CryoSat-2) thicker ice north of the Canadian Archipelago and north of Greenland than in 2012 and 2013. With the exception of the area east of Greenland which is of less interest for this study, strong differences between the posterior run and Cryosat-2 are restricted to the area north of Fram Strait towards the pole and the 2012 experiment. This residual misfit can be traced back to an inconsistency between observed ice concentration and thickness (and the model): as the simulated ice concentration in winter and spring in the Greenland Sea is too high (and, thus, the ice margin too far south) the assimilation responds by a reduction of ice thickness north of Fram Strait towards the pole, reflecting the pathway of the Transpolar Drift in the model. In other words: the prize we have to pay for a more reliable ice margin is a misfit to the CryoSat-2 ice thickness. Especially in March 2012 CryoSat-2 is showing very thick ice next to and along the described pathway (Fig. 6a) which is obviously not consistent with the model's ice margin (and ice dynamics).

As we assimilate only data in March and April, the observations for the subsequent months (when available) provide independent information that we can use to assess the forecast skill prior and posterior to the assimilation. Our skill score is the squared misfit weighted by the reciprocal of the squared uncertainty (as in the definition of the cost function, but without the extra scaling factor for the ice thickness contribution). For each experiment Fig. 7 shows the prior and posterior cost function contributions per data stream and month from March to December. In all experiments, for March and April (i.e. in the assimilation window) the contribution of CryoSat-2 is strongly reduced in the posterior run. In November, however, the skill of the posterior run is reduced for the 2012 and 2013 experiments, and only slightly increased for 2014. The skill for snow

depth simulation is strongly increased from March to June in 2012 and 2013, for 2014 is was already good in the prior. The period from July to September is less relevant, because there is little snow left. The skill for SST improves somewhat in March and April.

The posterior ice concentration has an increased skill in March and April. In the subsequent months the situation is mixed, at least Arctic-wide. We can, however, identify regions of increased and reduced skill as is illustrated by Fig. 8, which shows the September concentration misfit for the prior (row 1) and the posterior (row 2) simulations. For example, the skill in the Beaufort Sea and north of the Chukchi plateau is increased, while the skill over the Eurasian basin is decreased.

3.2 Reconstruction

Our next set of (three) experiments explores the feasibility of inferring an initial ice thickness distribution on 1 March that is consistent with the summer ice concentration for each of the years 2012 to 2014. We, hence, use an extended assimilation window from 1 March to 30 September and assimilate ice concentration from 1 July to 30 September together with snow depth and SST which we assimilate from March to September. We do not use any ice thickness observations. We use the same control vector as in the straightforward assimilation.

In each experiment the posterior March ice thickness exceeds the CryoSat-2 observations in large parts of the Arctic (see Fig. 6, rows 3 and 1). Areas with similar values as CryoSat-2 are the southern parts of the Beaufort Sea, the Chukchi Plateau, and the Kara and Laptev Seas. Over the Eurasian Basin slope except for areas north of the Laptev Sea the posterior ice thickness falls below CryoSat-2. Apparently high ice thickness values are required to match the ice concentration in summer which is shown in row 3 of Fig. 8. Note that, compared to the straightforward initialisation experiments here the ice margins are matching. Animations of ice thickness and concentration show that the improved match over the Eurasian Basin slope is caused by increased initial ice thickness north of the Laptev Sea (see row four in Fig. 6).

We can now compare our skill metrics, i.e. the cost function contributions per data stream and month from March to December (Fig. 9) with that for the straightforward initialisation (Fig. 7). The skill for ice concentration (panel b) is considerably increased from July to September (assimilated) but also from March to June (not assimilated). The skill is, however, already lost in October, probably because of the freezing of sea ice, which is not constrained by any satellite observations of the sea ice. Compared to the prior, the skill for Cryosat-2 data (panel a) is strongly reduced for March and April but only weakly reduced for November. The skill of snow depth is very similar to that of the straightforward initialisation. The fit to SST shows some improvement from May to August, compared to the prior and to the straightforward assimilation. This is probably an effect of the extended assimilation window, and maybe rather driven by observations of ice concentration than of SST.

3.3 Initialisation with bias correction

The ratio of the reconstructed and the CryoSat-2 ice thickness shows remarkable similarities of the three years (shown in Fig. 10 for March). We use this finding to derive a bias correction procedure: First, we average the ratio fields over the three years from 2012 to 2014 (shown in Fig. 11 for March and April). Second, we multiply the CryoSat-2 ice thickness for March and April by the corresponding ratio fields yielding bias-corrected Cryosat-2 ice thickness fields. Then we repeat the straightforward initialisation (described in Sect. 3.1) with the bias corrected CryoSat-2 fields.

The convergence of the minimisation is similar to that of the straightforward initialisation. The skill of the posterior concentration does, however, show a remarkable improvement until September (Fig. 12). The skill for SST is increased from March until July, and for snow depth it is very close to the straightforward initialisation (not shown). The misfit of the ice concentration in September is now strongly reduced for all years (row 4 of Fig. 8).

4 Conclusions

AWI's ocean–sea ice model NAOSIM has been recalibrated using observations from 1990 to 2008. We restricted the calibration to parameters which control the sea ice dynamics (but also the ocean dynamics) resulting in a horizontal ice thickness distribution much closer to the ICESat-JPL observations. A positive bias in the Beaufort Sea and a negative bias over the Eurasian Basin slope were strongly reduced. This is connected to a reduction of the ice drift speeds which are now much closer to the ice drift provided by OSI SAF and KIMURA. The horizontal ice thickness distribution for single events like the September 2007 sea ice minimum is also improved strongly. The time series of September sea ice extent and area are now much closer to the observations. While the standard version produces a minimum in extent and area in 1990 which almost reaches the 2007 values, the recalibrated model's 1990 simulation is much more realistic. This underlines the importance of a realistic horizontal ice thickness distribution to simulate extreme events correctly. The model is now able to reproduce the minima in 2007 and 2012 although the extent is somewhat overestimated. Also the long-term trend from 1980 to 2014 in extent and area is captured much better.

Subsequent data assimilation experiments use the following four data streams: CryoSat-2 sea ice thickness from AWI, sea ice concentration from OSI SAF, snow depth from University Bremen, and sea surface temperature (SST) from OSI SAF. Three assimilation experiments with these four data sets over an assimilation window covering March and April, for each of the years 2012 to 2014, were carried out and a forecast of the summer ice conditions was performed. To focus on the effect of constraining the initial state of the sea ice–ocean system, we assumed to have perfect seasonal atmospheric forecast providing perfect surface boundary conditions (for a use of this system in operational mode, uncertainty in boundary conditions can be handled through an ensemble approach). It turned out that the assimilation could only improve the summer conditions for some regions. Arctic-wide the forecast in summer could not be improved through the use of the sea ice and ocean observations in March and April.

A second set of experiments was used to construct an initial state that is consistent with the observational data sets except Cryosat-2 over a longer assimilation window from March to September. From this initial state we simulated the posterior ice thickness distribution in March and April. Since this set of experiments made use of the summer ice conditions, we called the inferred posterior ice thickness fields "reconstructed". The ratio of this "reconstructed" and the CryoSat-2 ice thickness fields for March and April is very similar for all three years. This allowed us to develop a bias correction scheme, which scales the CryoSat-2 ice thickness fields by the monthly three year average of the above ratio. Then we performed a third set of assimilation experiments for March and April similar to the first set of assimilations but used the above bias correction scheme for the CryoSat-2 ice thickness. This procedure yields a considerable improvement in forecast skill for sea ice from July to September for all three years. We note that our prediction target, namely the summer ice conditions of 2012 to 2014, have entered the assimilation procedure, because they were used to derive the ice thickness ratio in our bias correction scheme. However, the bias correction scheme can now also be applied to years beyond the period from 2012 to 2014. One of these applications is the Sea Ice Outlook 2015.

Acknowledgements. This work has been funded by the European Commission through its Seventh Framework Programme Research and Technological Development under contract number 265863 (ACCESS) through a grant to OASys and FastOpt.

References

AMAP: Snow, Water, Ice and Permafrost in the Arctic (SWIPA): Climate Change and the Cryosphere, Arctic Monitoring and Assessment Programme (AMAP), Oslo, Norway, 2011. 5522

Chevallier, M., and Salas-Mélia, D.: The Role of Sea Ice Thickness Distribution in the Arctic Sea Ice Potential Predictability: a Diagnostic Approach with a Coupled GCM, J. Climate, 25, 3025–3038, doi:10.1175/JCLI-D-11-00209.1, 2012. 5523

Chevallier, M., Salas y Melia, D., Voldoire, A., Déqué, M., and Garric, G.: Seasonal forecasts of the Pan-Arctic Sea ice extent using a GCM-based seasonal, J. Climate, 26, 6092–6104, doi:10.1175/JCLI-D-12-00612.1, 2013. 5523

Eastwood, S.: Atlantic High Latitude L3 Sea Surface Temperature Product User Manual Version 2.1, Technical Report, Norwegian Meteorological Institutes, Oslo, Norway, available at: http://osisaf.met.no/docs/osisaf_ss2_pum_ahl-sst_v2p1.pdf (last access: 28 November 2011), 2011a. 5528

Eastwood, S.: Validation Report for the Atlantic High Latitude L3 Sea Surface Temperature product Version 1.0, Technical Report osi-203, Norwegian Meteorological Institutes, Oslo, Norway, available at: http://osisaf.met.no/docs/val_hlsst_n16.pdf (last access: 26 April 2011), 2011b. 5528

Eastwood, S., Jenssen, M., Lavergne, T., Sorensen, A., and Tonboe, R.: EUMETSAT Ocean and Sea Ice Satelitte Application Facility. Global sea ice concentration reprocessing product (v1.2), Product user manual, Technical Report, Norwegian and Danish Meteorological Institutes, Oslo, Norway and Copenhagen, Denmark, 2015. 5526, 5528

Gerdes, R., Karcher, M. J., Kauker, F., and Schauer, U.: Causes and development of repeated Arctic Ocean warming events, Geophys. Res. Lett., 30, 1980, doi:10.1029/2003GL018080, 2003. 5524

Giering, R. and Kaminski, T.: Recipes for adjoint code construction, ACM Trans. Math. Software, 24, 437–474, 1998. 5525

Harder, M.: Dynamics, roughness, and age of Arctic sea ice – numerical investigations with a large-scale model, Ber. polarforsch., Alfred Wegener Institute, Bremerhaven, Germany, 1996. 5529

Holland, M. M. and Stroeve, J.: Changing seasonal sea ice predictor relationships in a changing Arctic climate, Geophys. Res. Lett., 38, L18501, doi:10.1029/2011GL049303, 2011. 5523

Kaleschke, L., Tian-Kunze, X., Maaß, N., Mk¨ynen, M., and Drusch, M.: Sea ice thickness retrieval from SMOS brightness temperatures during the Arctic freeze-up period, Geophys. Res. Lett., 39, L05501, doi:10.1029/2012GL050916, 2012. 5525

Kalnay, E., Kanamitsu, M., Kistler, R., Collins, W., Deaven, D., Gandin, L., Iredell, M., Saha, S., White, G., Woollen, J., Zhu, Y., Leetmaa, A., Reynolds, R., Chelliah, M., Ebisuzaki, W., Higgins, W., Janowiak, J., Mo, K. C., Ropelewski, C., Wang, J., Jenne, R., and Joseph, D.: The NCEP/NCAR 40-year reanalysis project, B. Am. Meteorol. Soc., 77, 437–471, 1996. 5530

Kauker, F., Gerdes, R., Karcher, M., Köberle, C., and Lieser, J.: Variability of Arctic and North Atlantic sea ice: a combined analysis of model results and observations from 1978 to 2001, J. Geophys. Res.-Oceans, 108, 3182, doi:10.1029/2002JC001573, 2003. 5524, 5529, 5530

Kauker, F., Kaminski, T., Karcher, M., Giering, R., Gerdes, R., and Voßbeck, M.: Adjoint analysis of the 2007 all time Arctic sea-ice minimum, J. Geophys. Res., 36, L03707, doi:10.1029/2008GL036323, 2009. 5523, 5525

Kimura, N., Nishimura, A., Tanaka, Y., and Yamaguchi, H.: Influence of winter sea-ice motion on summer ice cover in the Arctic, Polar Res., 32, 20193, doi:10.3402/polar.v32i0.20193, 2013. 5527

Köberle, C. and Gerdes, R.: Mechanisms determining the variability 2003: mechanisms determining the variability of Arctic sea ice conditions and export, J. Climate, 16, 2843–2858, 2003. 5529

Kurtz, N. T., Richter-Menge, J., Farrell, S., Studinger, M., Paden, J., Sonntag, J., and Yungel, J.: IceBridge airborne survey data support arctic sea ice predictions, EOS Trans. AGU, 94, doi:10.1002/2013eo040001, 2013a. 5529

Kurtz, N. T., Farrell, S. L., Studinger, M., Galin, N., Harbeck, J. P., Lindsay, R., Onana, V. D., Panzer, B., and Sonntag, J. G.: Sea ice thickness, freeboard, and snow depth products from Operation IceBridge airborne data, The Cryosphere, 7, 1035–1056, doi:10.5194/tc-7-1035-2013, 2013b. 5529

Kwok, R. and Cunningham, G. F.: ICESat over Arctic sea ice: Estimation of snow depth and ice thickness, Geophys. Res. Lett., 113, C08010, doi:10.1029/2008JC004753, 2008. 5526

Lavergne, T., Eastwood, S., Teffah, Z., Schyberg, H., and Breivik, L.-A.: Sea ice motion from low-resolution satellite sensors: An alternative method and its validation in the Arctic, J. Geophys. Res.-Oceans, 115, C10032, doi:10.1029/2009JC005958, 2010. 5526

Lindsay, R., Haas, C., Hendricks, S., Hunkeler, P., Kurtz, N., Paden, J., Panzer, B., Sonntag, J., Yungel, J., and Zhang, J.: Seasonal forecasts of Arctic sea ice initialized with observations of ice thickness, Geophys. Res. Lett., 39, L21502, doi:10.1029/2012GL053576, 2012. 5523

Lindsay, R., Wensnahan, M., Schweiger, A., and Zhang, J.: Evaluation of seven different atmospheric reanalysis products in the Arctic, J. Climate, 27, 2588–2606, doi:10.1175/JCLI-D-13-00014.1, 2014. 5531

Markus, T. and Cavalieri, D.: Snow depth distribution over Sea Ice in the Southern Ocean from satellite passive microwave data, in: Antarctic Sea Ice: Physical Processes, Interactions and

Variability, no. 74 in Antarctic Research Series, edited by: Jeffries, M., American Geophysical Union, AGU, Washington, D.C., 19–39, 1998. 5528

Massonnet, F., Fichefet, T., and Goosse, H.: Prospects for improved seasonal Arctic sea ice predictions from multivariate data assimilation, Ocean Model., 88, 16–25, 2015. 5523

Ricker, R., Hendricks, S., Helm, V., Skourup, H., and Davidson, M.: Sensitivity of CryoSat-2 Arctic sea-ice freeboard and thickness on radar-waveform interpretation, The Cryosphere, 8, 1607–1622, doi:10.5194/tc-8-1607-2014, 2014. 5526, 5528

Saha, S., Moorthi, S., Pan, H., Wu, X., Wang, J., Nadiga, S., Tripp, P., Kistler, R., Woollen, J., Behringer, D., Liu, H., Stokes, D., Grumbine, R., Gayno, G., Wang, J., Hou, Y., Chuang, H., Juang, H. H., Sela, J., Iredell, M., Treadon, R., Kleist, D., Van Delst, P., Keyser, D., Derber, J., Ek, M., Meng, J., Wei, H., Yang, R., Lord, S., van den Dool, H., Kumar, A., Wang, W., Long, C., Chelliah, M., Xue, Y., Huang, B., Schemm, J., Ebisuzaki, W., Lin, R., Xie, P., Chen, M., Zhou, S., Higgins, W., Zou, C., Liu, Q., Chen, Y., Han, Y., Cucurull, L., Reynolds, R. W., Rutledge, G., and Goldberg, M.: The NCEP Climate Forecast System Reanalysis, B. Am. Meteorol. Soc., 91, 1015–1057, doi:10.1175/2010BAMS3001.1, 2010. 5529

Saha, S., Moorthi, S., Wu, X., Wang, J., Nadiga, S., Tripp, P., Behringer, D., Hou, Y., Chuang, H., Iredell, M., Ek, M., Meng, J., Yang, R., Peña Mendez, M., van den Dool, H., Zhang, Q., Wang, W., Chen, M., and Becker, E.: The NCEP Climate Forecast System Version 2, J. Climate, 27, 2185–2208, doi:10.1175/JCLI-D-12-00823.1, 2014. 5529

Sakov, P., Counillon, F., Bertino, L., Lisæter, K. A., Oke, P. R., and Korablev, A.: TOPAZ4: an ocean-sea ice data assimilation system for the North Atlantic and Arctic, Ocean Sci., 8, 633–656, doi:10.5194/os-8-633-2012, 2012. 5531

Schweiger, A., Lindsay, D., Zhang, J., Steele, M., and Stern, H.: Uncertainty in modeled arctic sea ice volume, J. Geophys. Res., 117, C00D06, doi:10.1029/2011JC007084, 2011. 5531

Sigmond, M., Fyfe, J., Flato, G., Kharin, V., and Merryfield, W.: Seasonal forecast skill of Arctic sea ice area in a dynamical forecast system, Geophys. Res. Lett., 40, 529–534, 2013. 5523

Steele, M., Morley, R., and Ermold, W.: PHC: A global ocean hydrography with a high-quality Arctic Ocean, J. Climate, 14, 2079–2087, 2001. 5530

Stroeve, J., Holland, M. M., Meier, W., Scambos, T., and Serreze, M.: Arctic sea ice decline: faster than forecast, Geophys. Res. Lett., 34, L09501, doi:10.1029/2007GL029703, 2007. 5522

Stroeve, J., Hamilton, L. C., Bitz, C. M., and Blanchard-Wrigglesworth, E.: Predicting September sea ice: ensemble skill of the SEARCH sea ice outlook 2008–2013, Geophys. Res. Lett., 41, 2411–2418, 2014. 5523

Sumata, H., Girard-Ardhuin, T. L. F., Kimura, N., Tschudi, M., Kauker, F., Karcher, M., and Gerdes, R.: An intercomparison of Arctic ice drift products to deduce uncertainty estimates, J. Geophys. Res.-Oceans, 119, 4887–4921, doi:10.1002/2013JC009724, 2014. 5527

Sumata, H., Kwok, R., Gerdes, R., Kauker, F., and Karcher, M.: Uncertainty of Arctic summer ice drift assessed by high-resolution SAR data, J. Geophys. Res.-Oceans, 120, 5285–5301, doi:10.1002/2015JC010810, 2015. 5527

Wang, W., Chen, M., and Kumar, A.: Seasonal prediction of arctic sea ice extent from a coupled dynamical forecast system, Mon. Weather Rev., 141, 1375–1394, doi:10.1175/MWR-D-12-00057.1, 2013. 5523

Wingham, D., Francis, C., Baker, S., Bouzinac, C., Brockley, D., Cullen, R., de Chateau-Thierry, P., Laxon, S., Mallow, U., Mavrocordatos, C., Phalippou, L., Ratier, G., Rey, L., Rostan, F., Viau, P., and Wallis, D. W.: CryoSat: a mission to determine the fluctuations in Earth's land and marine ice fields, Adv. Space Res., 37, 841–871, doi:10.1016/j.asr.2005.07.027, 2006. 5525

Yang, Q., Losa, S., Losch, M., Tian-Kunze, X., Nerger, L., Liu, J., Kaleschke, L., and Zhang, Z.: Assimilating SMOS sea ice thickness into a coupled ice–ocean model using a local SEIK filter, J. Geophys. Res., 119, 6680–6692, doi:10.1002/2014JC009963, 2014. 5523

Zhang, J. and Rothrock, D. A.: Modeling global sea ice with a thickness and enthalpy distribution model in generalized curvilinear coordinates, Mon. Weather Rev., 131, 845–861, 2003. 5531

Zhang, J., Steele, M., Lindsay, R., Schweiger, A., and Morison, J.: Ensemble 1-year predictions of Arctic Sea ice for the spring and summer of 2008, Geophys. Res. Lett., 35, L08502, doi:10.1029/2008GL033244, 2008. 5523

Zwally, H., Yi, D., Kwok, R., and Zhao, Y.: ICESat measurements of sea ice freeboard and estimates of sea ice thickness in the Weddell Sea, J. Geophys. Res., 113, C02S15, doi:10.1029/2007JC004284, 2008. 5526, 5544

Table 1. The costfunction for the three data streams separated by winter and summer (columns 2 to 7), the sum of the terms (column 8), and the normalized sum (column 9) for standard NAOSIM (NAOSIM) and the recalibrated NAOSIM (newNAOSIM). Additionally, the costfunction with respect to the ICESAT thickness and ice drift is given for PIOMAS2.1 and TOPAZ4.

Model	concn. Nov–Apr	concn. May–Oct	ICESAT Feb/Mar	ICESAT Oct/Nov	drift Oct–Apr	drift May–Jul	total	weighted
NAOSIM	234 429	430 621	3550	3753	120 959	126 750	920 063	3.00
newNAOSIM	405 000	405 221	1793	1664	22 689	38 131	963 117	1.94
PIOMAS2.1	–	–	1383	1125	46 231	67 254	–	–
TOPAZ4	–	–	2949	2276	159 021	109 079	–	–

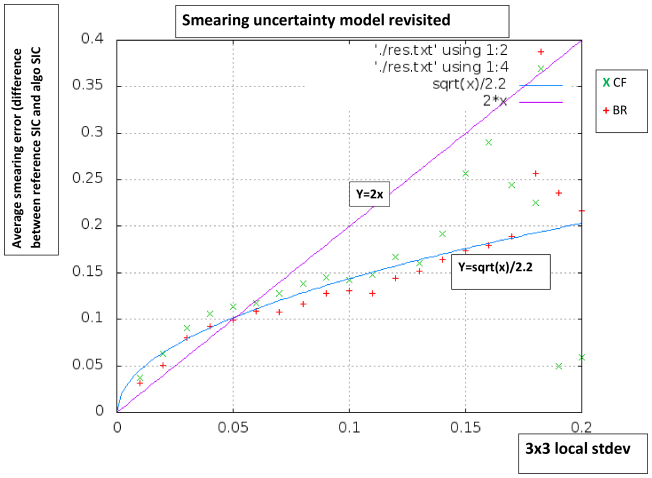

Figure 1. The empirical fit of the smearing uncertainty. Root mean squared difference between high resolution SIC aggregated to 10 km resolution (reference) and that computed at the SSMI footprints using the Comiso Frequency mode (CF, green crosses) or the BRistol (BR, red crosses) algorithms (which are applied in the OSISAF algorithm).

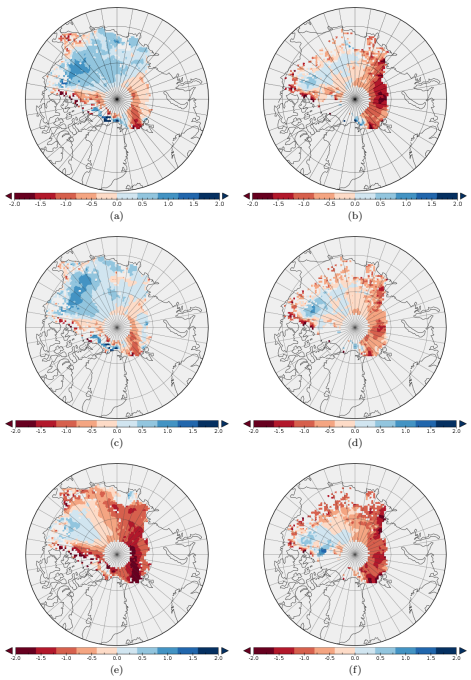

Figure 2. The difference of the modelled and observed (ICESat-JPL) ice thickness climatology [m] for February/March (left) and October/November for newNAOSIM **(a, b)**, PIOMAS2.1 **(c, d)**, and TOPAZ4 **(e, f)** for the mean from 2003–2008. Only points where the deviation of ICESat-JPL from ICESAT-GSFC (Zwally et al., 2008) is below 40 cm are used.

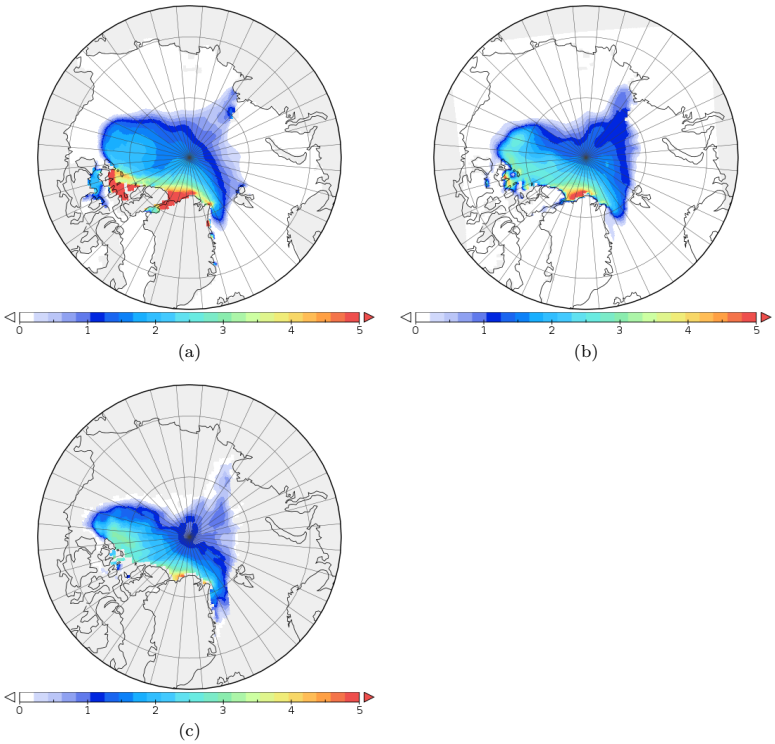

Figure 3. The sea ice thickness [m] September 2007 as simulated by **(a)** newNAOSIM, **(b)** PIOMAS 2.1, and **(c)** TOPAZ4.

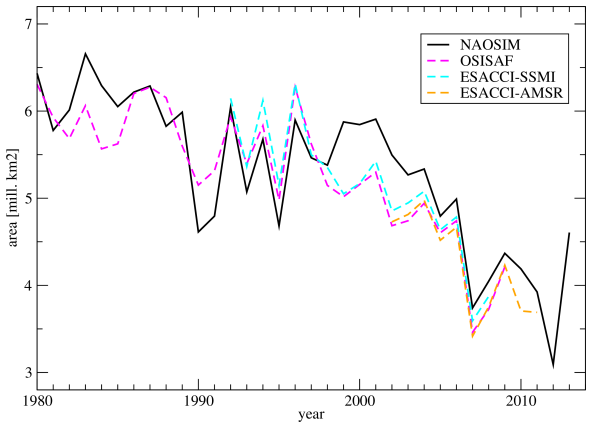

Figure 4. The September sea ice area of newNAOSIM (black) and three estimates based on remotely sensed ice concentration (dashed). OSI SAF (re-processed) and SICCI based on two different sensors (SMMR/SSMI and AMSR, available from http://icdc.zmaw.de/esa-cci_sea-ice-ecv0.html).

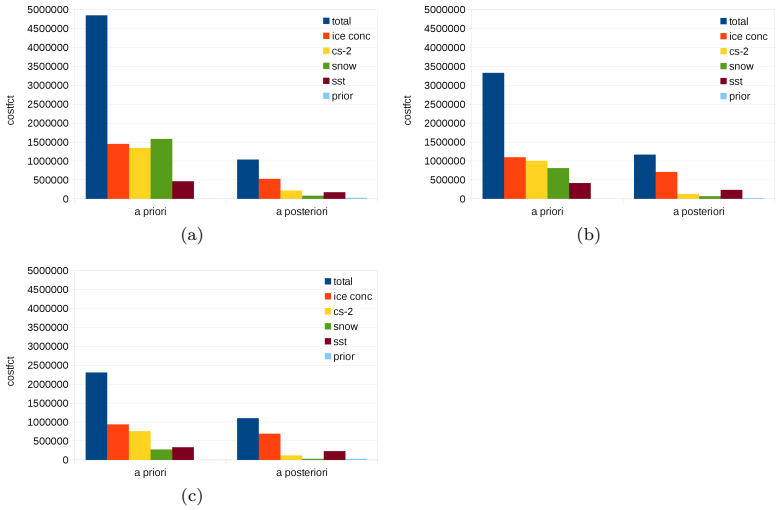

Figure 5. The terms of the cost function before and after the optimization for **(a)** 2012, **(b)** 2013, **(c)** 2014.

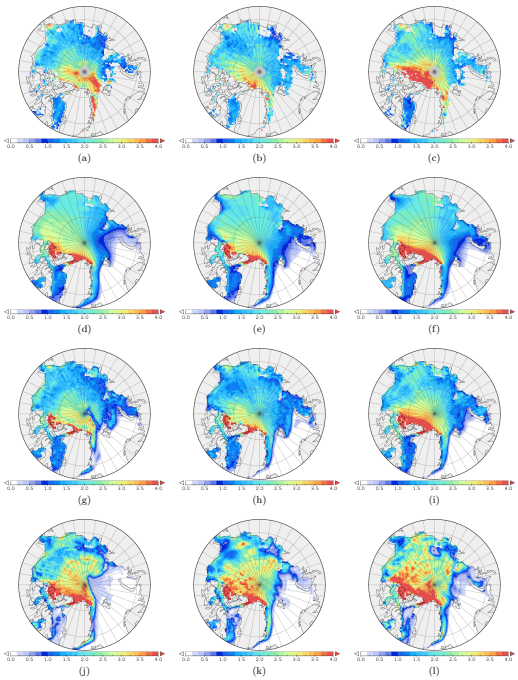

Figure 6. The ice thickness [m] of the CryoSat-2 product (top row); ice thickness of new-NAOSIM prior to the assimilation (second row), after the straightforward assimilation (third row), and after the reconstruction (fourth row) for March 2012 **(a, d, g, j)**, March 2013 **(b, e, h, k)**, and March 2014 **(c, f, i, l)**.

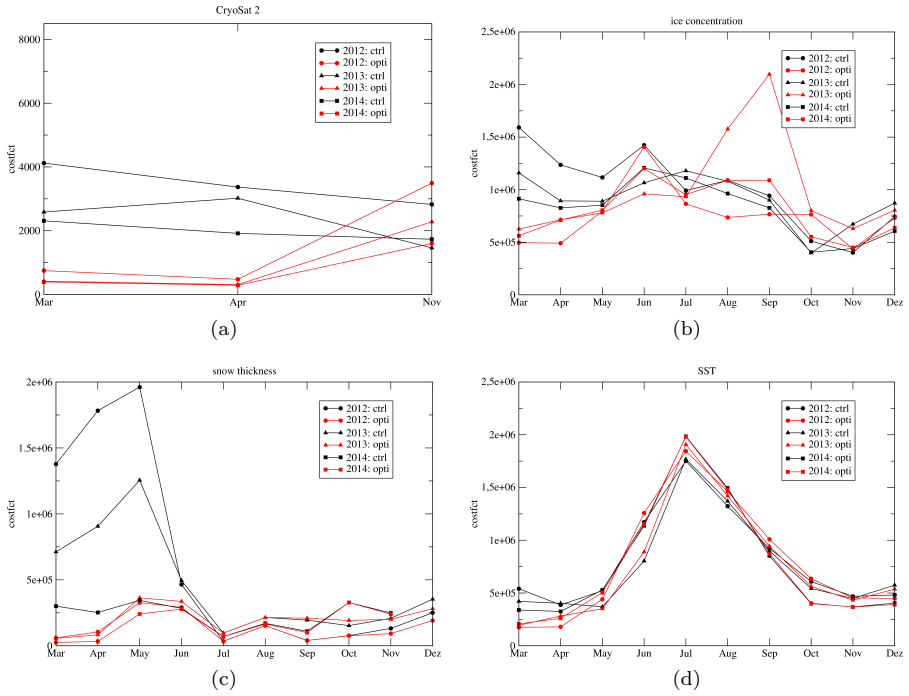

Figure 7. Prior and posterior misfit per data stream and month from **(a)** the CryoSat-2 ice thickness (data are currently only available for March, April and November; not scaled, see text), **(b)** the OSI SAF ice concentration, **(c)** the snow depth (UB), and **(d)** the OSI SAF SST.

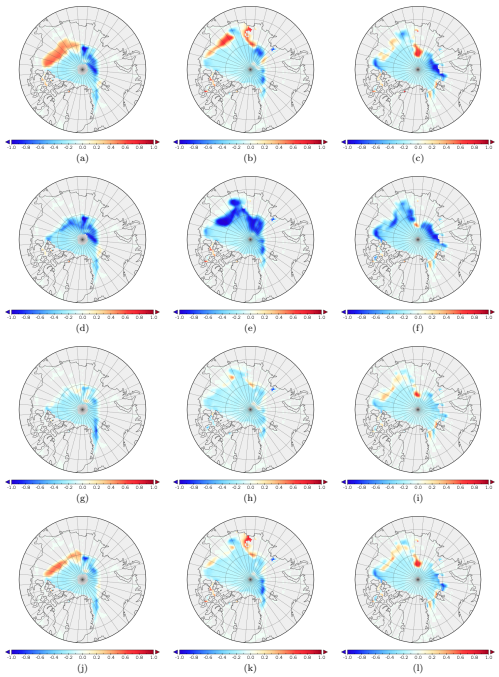

Figure 8. The misfit between simulated and OSI SAF ice concentration prior to (top row), after the straightforward assimilation (second row), after the reconstruction (third row), and after the bias-corrected assimilation (fourth row) and the OSI SAF ice concentration for September 2012 **(a, d, g, j)**, September 2013 **(b, e, h, k)**, and September 2014 **(c, f, i, l)**.

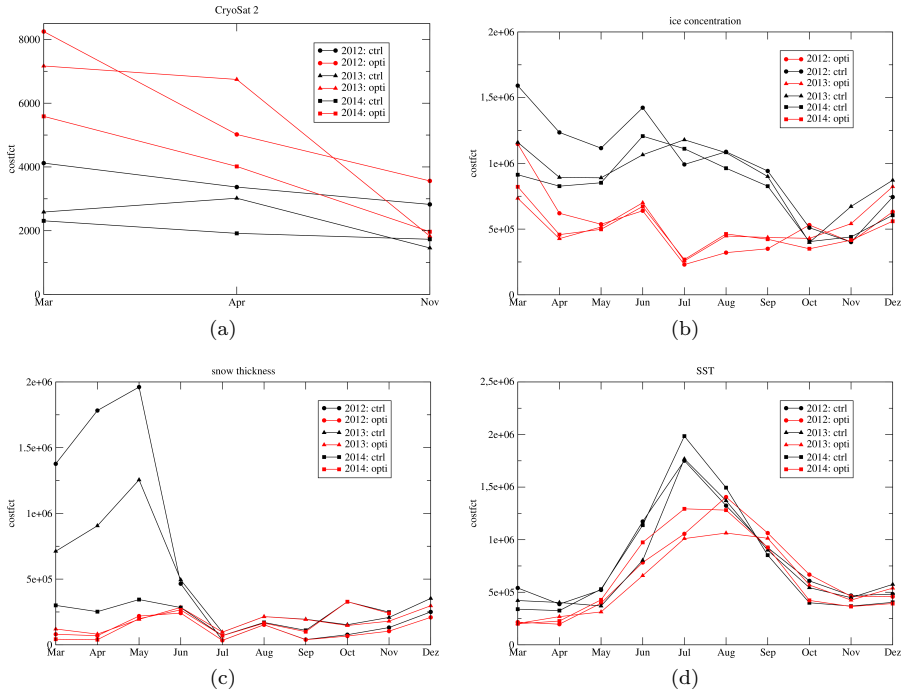

Figure 9. As Fig. 7 but for the reconstruction experiment.

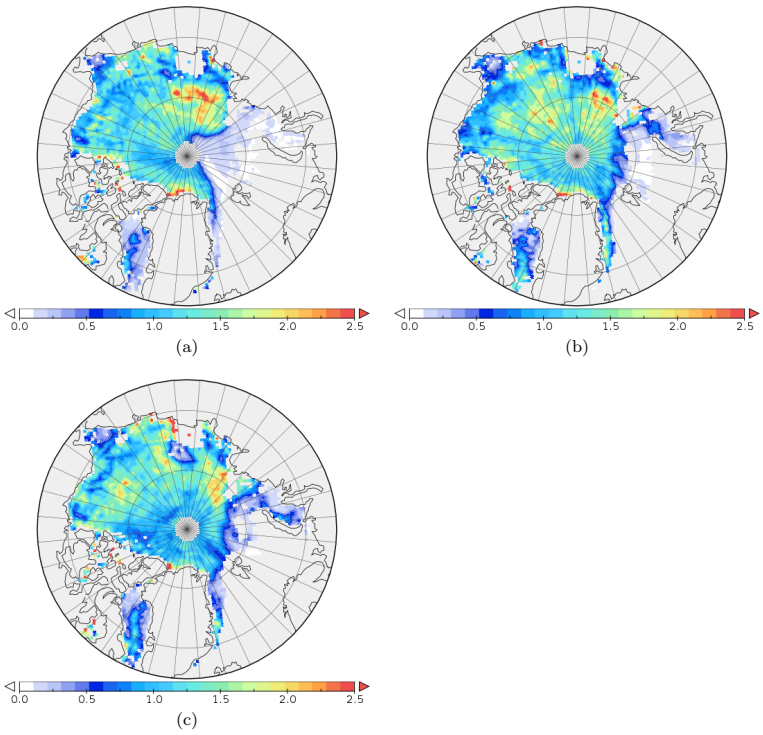

Figure 10. The ratio of the reconstructed and the CryoSat-2 ice thickness **(a)** March 2012, **(b)** March 2013, and **(c)** March September 2014.

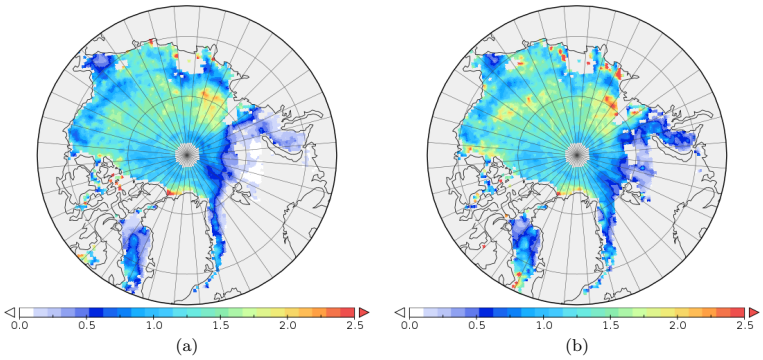

Figure 11. The mean ratio for **(a)** March and **(b)** April.

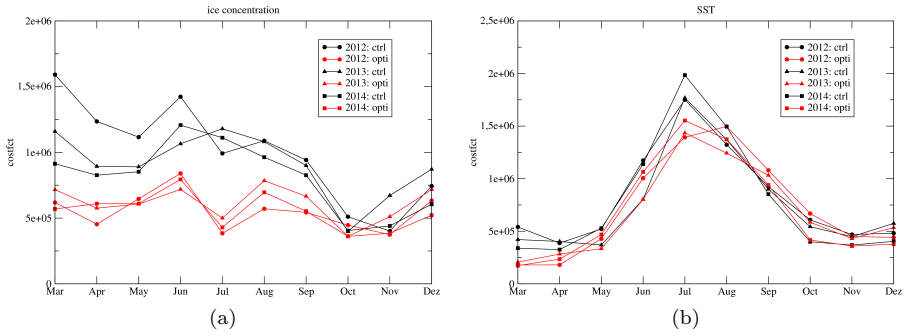

Figure 12. As Fig. 7 but for the bias-corrected assimilation experiment. Only the misfit of the ice concentration and SST are shown.